# Phase-Change Memory Simulations Using an Analytical Phase Space Model

Bernhard Schmithusen
Synopsys Switzerland LLC
Zurich, Switzerland
schmithu@synopsys.com

Pavel Tikhomirov
Synopsys Switzerland LLC
Zurich, Switzerland
pavelt@synopsys.com

Eugeny Lyumkis
Synopsys Inc.
Mountain View, CA, US
eugeny@synopsys.com

***Abstract*—In this paper, an analytical phase transition model is coupled self-consistently with the electro-thermal transport model. The phase space model and the transition dynamic is described. The resulting phase-electro-thermal simulation model is applied to an illustrative example structure. The self-consistency of the approach and its resulting simulation speed and robustness provide a useful TCAD tool for design studies of phase change memory devices.**

## I. INTRODUCTION

Phase change memory (PCM) is an emerging technology for non-volatile memory devices. The device operation relies on reversible changes of the phases of chalcogenide materials such as $Ge_2Sb_2Te_5$ (GST). At room temperature two phases, a crystalline and an amorphous one, are observed in practice and exhibit different conductivities which are used to establish the memory effect (READ). Switching crystalline to amorphous phase (RESET) is performed electronically by applying a short but sufficiently large current pulse, which causes the material to melt. After pulse end, the temperature decreases rapidly, the GST solidifies, but has no time to crystallize again and remains amorphous. The transition from amorphous to crystalline (SET) is done with a smaller pulse where the temperature does not reach the melting temperature and crystallization takes place.

Modeling of the fundamental operations RESET, SET, and READ, is a challenging task and includes the modeling of phase transitions coupled with the electro-thermal properties of the device. In this paper, an analytical phase transition model is coupled self-consistently with the electro-thermal transport model.

There is a considerable number of studies in the literature to model physical mechanisms of amorphization and crystallization processes [1]–[4]. These models are very useful in helping to understand the physical phenomena. For practical applications more appropriate might be a simple TCAD-oriented approach, which guarantees speed and robustness of simulation, provides an easy way to calibrate realistic structures, and allows easy parameter variations. The analytical phase transition model presented in this paper is based on kinetic equations describing transition between phases; kinetic equations are coupled self-consistently with electro-thermal transport models available in general purpose device simulators, which allows simulation of arbitrary 2D or 3D geometries.

## II. PHASE SPACE MODEL

Our approach models phases as continuous volume fractions $s_i$ and describes the phase dynamic by analytical transition rates. Given a fixed number of different phases, one has $\sum_i s_i = 1$ with $s_i \geq 0$. The dynamic between phases is locally described by

$$\dot{s_i} = \sum_{j \neq i} \sum_{t \in T_{ij}} (c_t s_j - e_t s_i)$$

where $t \in T_{ij}$ is a transition process between the phases $i$ and $j$, and $c_t$ and $e_t$ appropriate forward and backward reaction rates, respectively. Here, the rates depend on the state of the electro-thermal system, especially on the lattice temperature.

We consider three different phases, namely crystalline, amorphous, and melt. In classical nucleation theory [5], the phase transition from amorphous to crystalline is described by nucleation and growth processes of the nuclei. Nucleation is described by the probability of an amorphous monomer to crystallize [1], [3], [4] which can be directly translated into local reaction rates of our model. Hence, in analogy to the nucleation probabilities of [1] and [4], we introduce an amorphous to crystalline reaction rate of the form

$$\begin{aligned} c_N &= r_0^N \exp(-\beta(E_{\text{act}^N} + \Delta G^*(T))) \\ \Delta G^*(T) &= \frac{16}{3}\pi {\gamma_{\text{SL}}}^3 / \Delta G(T)^2 \end{aligned}$$

where $r_0^N$ is the frequency factor of the process ‘N’, $1/\beta = kT$, $E_{\text{act}}^N$ the activation energy of ‘N’, $\Delta G^*$ the temperature dependent nucleation barrier, which depends on the bulk free energy density (per volume) $\Delta G$ of undercooled liquid and solid phases and the interfacial free energy $\gamma_{\text{SL}}$ of the phases.

In kinetic models of crystallization, the growth process is described by growth velocities of the crystalline nuclei [1], [4], i.e. the transformations depend on nonlocal properties. As the reaction rates of our model are restricted to local dependencies, growth is modeled by

$$c_G = r_0^G \exp(-\beta E_{\text{act}}^G)[1 - \exp(-\beta \Delta G(T))]$$

which partly reflects properties of the growth velocities.

978-1-4244-1753-7/08/$25.00 ©2008 IEEE

In most PCM modeling approaches, the melt phase is the only one existing above melting temperature. We assume that the transition from melt to amorphous is fast and temperature independent, while the melt to crystalline reaction rate follows an Arrhenian law.

## III. Electro-Thermal Model

We describe the phase change material as a semiconductor, and transport therein with the drift-diffusion equations. We model the impact of the phase composition by phase dependent band structure and transport parameters.

We assume that the current is carried by holes and introduce p-doping to match reported electronic conductivities for the crystalline GST [1]. To achieve the strong phase dependence of the conductivity, both the band structure and the carrier mobilities are phase dependent. Firstly, the phases affect the transport by modifying the carrier densities $p$ by means of an band edge shift $\Lambda_p$, i.e. $p = N_\mathrm{V}\mathcal{F}((E_\mathrm{V} - E_{\mathrm{F}_p} - \Lambda_p)/kT)$ with $N_\mathrm{V}$ the effective density-of-states, $E_\mathrm{V}$ the valence band energy, $E_{\mathrm{F}_p}$ the hole quasi-Fermi energy, and $\mathcal{F}$ the Fermi integral of order 1/2. $\Lambda_p$ is proportional to the non-crystalline phase fraction and reduces the carrier densities. Secondly, The hole mobility for the amorphous phase at room temperature is chosen two orders of magnitude smaller than for the crystalline phase, while electron mobilities are kept constant.

It has been observed that conductivities of the amorphous and crystalline GST are identical at temperatures above the glass temperature of the material [1]. To account for this behavior, above glass temperature $T_\mathrm{g} = 653\,\mathrm{K}$, we assume that the band edge shift vanishes and amorphous hole mobility reaches the crystalline value. Hence, above glass temperature, the transport parameters are regarded as phase independent.

Due to our phase space model, where phases are given as volume fractions, transport parameters have to be averaged as a function of the the phase fractions, referred to as the percolation effect. For simplicity, mobilities in a mixed phase state are interpolated linearly between the crystalline and non-crystalline phases.

The thermal behavior of the device is described by the lattice heat equation. The thermal model takes the electron and hole Joule heat into account.

Different to approaches reported in the literature, where the kinetic of phase transitions is described on meshes reflecting the size of crystallization monomers or nuclei of critical size, here the same mesh is employed for both the electro-thermal system and the phase kinetics. The analytical formulation allows a completely self-consistent solution of the fully coupled phase-electro-thermal system.

TABLE I
THERMAL MODEL PARAMETER.

| Material | $\kappa$ [W/(K cm)] | $c_V$ [J/(K cm$^3$)] |
|---|---|---|
| TiN | 0.13 | 3.235 |
| heater (TiN) | 0.01 | 0.3235 |
| W | 1.75 | 2.58 |
| $SiO_2$ | 0.005 | 1.67 |
| GST | 0.005 | 1.3 |

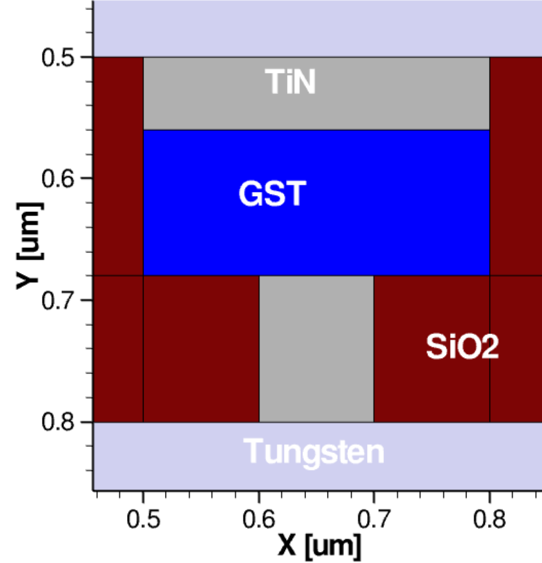

Fig. 1. Example PCM structure.

## IV. Application to Example PCM Structure

Our example PCM device, similar to the one of [1], is depicted in Fig.1. The material parameters for the nucleation rate are taken from the same reference, while all other parameters for the phase dynamic have been chosen heuristically. According to the electrical model in [2], we have chosen for the pure non-crystalline phase a band edge shift of 0.2 eV. The hole mobilities in the crystalline and non-crystalline phase take the values 15 $\mathrm{cm}^2/\mathrm{Vs}$ and 0.15 $\mathrm{cm}^2/\mathrm{Vs}$, respectively, while the phase independent electron mobility is 0.1 $\mathrm{cm}^2/\mathrm{Vs}$. The thermal parameters for the surrounding materials are chosen as

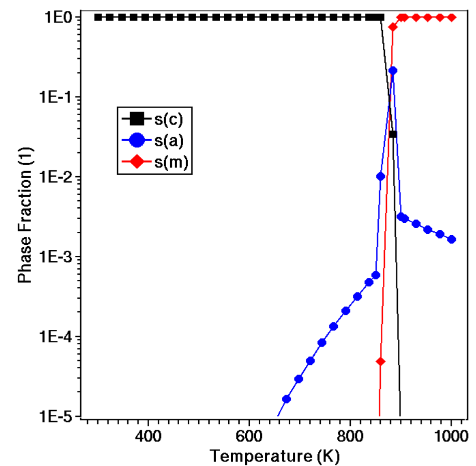

Fig. 2. The equilibrium phase fractions.

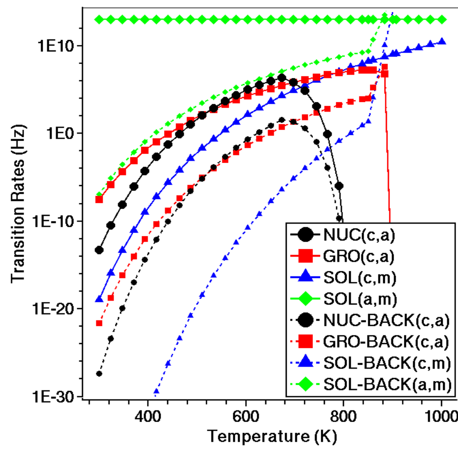


Fig. 3. Transition rates of the phase space model.

in [1], but due to the fact, that here the structure is simulated in 2D, the thermal conductivities and heat capacitances for the heater and oxide are slightly reduced.

In thermal equilibrium (Fig.2), the crystalline and melt phase are the dominant phases below and above melting temperature, respectively, while the amorphous phase is unstable over the whole temperature range. The melting temperature of the crystal is at about 889 K. All transitions are considered with their corresponding back reaction rates and satisfy the detailed balance principle (Fig.3).

We apply a RESET operation and a subsequent SET operation to the device (Fig. 4). The RESET pulse starts at $t = 0\,\mathrm{s}$ and consists of a 3 mA current pulse of 20 ns duration, while the SET current pulse inserts at $t = 160\,\mathrm{ns}$, has a size of 1.5 mA, and lasts 1000 ns. It can be seen that the crystalline volume fraction decreases under the RESET

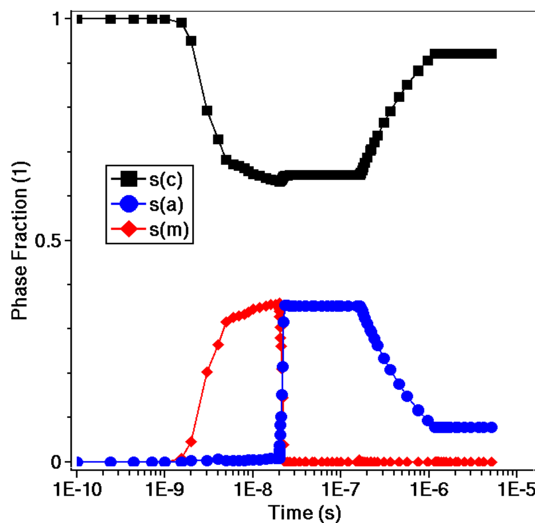


Fig. 4. RESET and SET operation: phase volume fractions of whole GST region as a function over time, where a RESET and SET operation is performed.

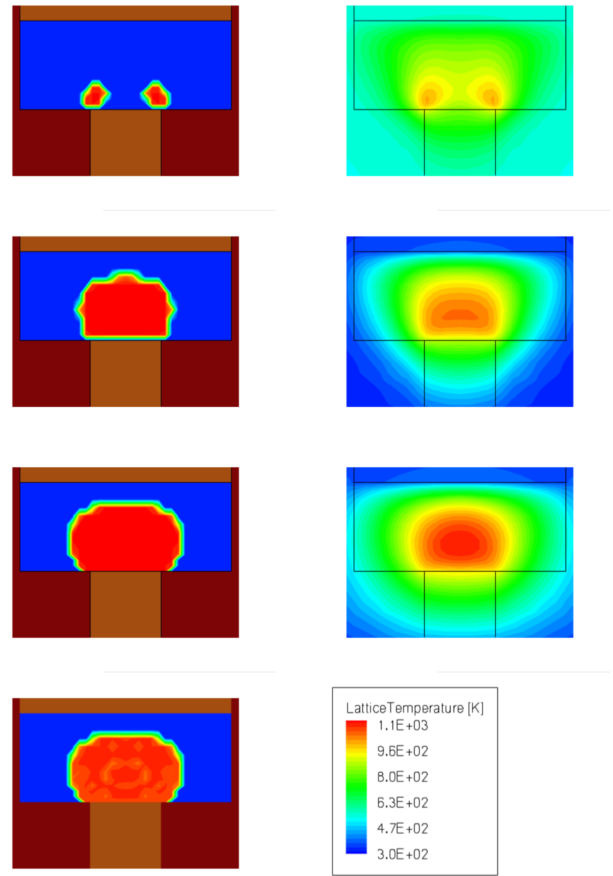


Fig. 5. RESET operation: non-crystalline phase fraction (left) and temperature (right) at 2 ns, 4 ns, 20 ns, and 160 ns after start of RESET pulse.

pulse for the benefit of the melt fraction, while the amorphous phase remains insignificant. During quenching, after the end of RESET, a small part of the material recrystallizes and the melt phase transforms almost completely to the amorphous one. With the insertion of the SET pulse, a large part of the device recrystallizes.

The spatial onset of melting and the evolving shape of the non-crystalline spot under RESET is depicted in Fig. 5. The non-crystalline spot is created at the beginning close at the heater-insulator interface (2 ns), evolves into the center above the heater, but still away from the interface (4 ns), covers at the end of RESET complete the heater contact (20 ns), and ends, after quenching, with the same shape but slightly reduced volume fraction. The spatial evolution of the spot depend strongly on the thermal properties of the materials and interfaces and the phase kinetics.

During the SET operation, the material recrystallizes which is depicted in Fig. 6. Depending on the dynamic behavior of the temperature profile, areas of the device might remain partly in the amorphous phase.

The READ operation is performed by a transient ramp up to 0.1 mA in 1 ms and results are depicted in Fig. 7 for the resulting RESET and SET devices, as well as the pure

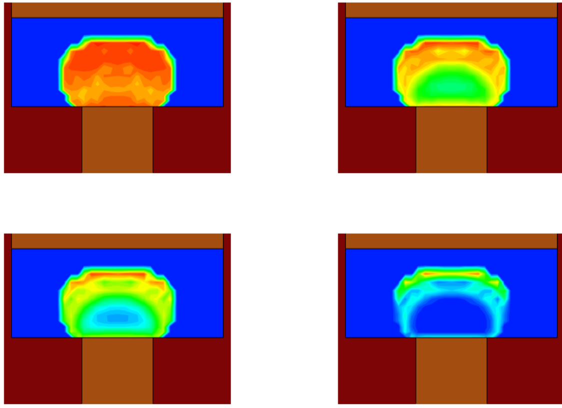

Fig. 6. SET operation: non-crystalline phase fraction at 20 ns, 100 ns, 200 ns, and 1000 ns after start of SET pulse.

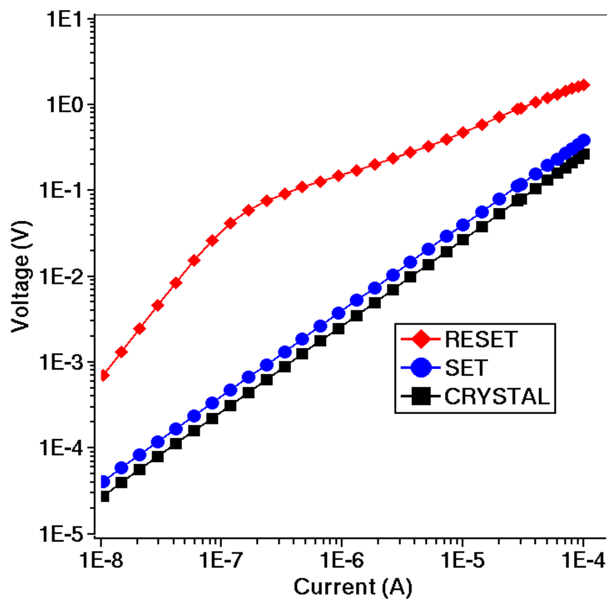


Fig. 7. READ operation: V-I characteristic of transient read operation for RESET, SET, and pure crystalline structure.

crystalline device as reference. The SET resistivity is close to that of pure crystalline. The observed resistivity change for the RESET device maximally increases by more than 2 orders of magnitudes at a current of 0.1 $\mu$A. For smaller currents, the low observed resistivity of the RESET device is due to capacitance effects, while for larger values an exponential decay occurs as reported in [6], due to the valence band edge shift.

Simulation times for the complete RESET and SET cycle on a single Intel Xeon processor with a CPU clock frequency of 3 GHz are typically less than one hour for reasonable grid sizes.

## V. Conclusions

Our approach is a flexible framework for the simulation of phase change memory devices coupling standard electro-thermal transport models for semiconductor devices with an analytical phase space model. It has been integrated into Sentaurus Device [7], supporting advanced electro-thermal transport models and arbitrarily shaped device structures in 2D and 3D. The analytical formulation of the approach leads to numerical robustness and high simulation speed, which are important for intensive design studies where wide model parameter ranges have to be covered.

## Acknowledgment


The authors gratefully acknowledge Andreas Wettstein for multiple fruitful discussions and invaluable advice.


## References


[1] D.-H. Kim, F. Merget, M. Först, and H. Kurz, “Three-dimensional simulation model of switching dynamics in phase change random access memory cells,” *J. Appl. Phys.*, vol. 101, pp. 1–12, 2007 (online).

[2] A. Pirovano, A. L. Lacaita, A. Benvenuti, F. Pellizzer, and R. Bez, “Electronic switching in phase-change memories,” *IEEE Trans. Elec. Dev.*, vol. 51, no. 3, pp. 452–459, Mar. 2004.

[3] S. Senkader and C. D. Wright, “Models for phase-change of $Ge_2Sb_2Te_2$ in optical and electrical memory devices,” *J. Appl. Phys.*, vol. 95, no. 2, pp. 504–511, 2004.

[4] C. Peng, L. Cheng, and M. Mansuripur, “Experimental and theoretical investigations of laser-induced crystallization and amorphization in phase-change optical recording media,” *J. Appl. Phys.*, vol. 82, no. 9, pp. 4183–4191, Nov. 1997.

[5] D. A. Porter and K. E. Easterling, *Phase Transformations in Metals and Alloys*. Stanley Thornes, Cheltenham, 1992.

[6] A. Redaelli, A. L. Lacaita, A. Benvenuti, and A. Pirovano, “Comprehensive numerical model for phase-change memory simulations,” in *SISPAD 2005*, 2005, pp. 279–282.

[7] *Sentaurus Device User Guide*, Synopsys Inc., 2008.